

Revisiting the definition of rapid intensification of tropical cyclones by clustering the initial intensity and inner-core size

Yi Li^{1,2,3}, Youmin Tang^{3,4,5}, Ralf Toumi⁶, Shuai Wang^{6,7}

¹Key Laboratory of Marine Hazards Forecasting, Ministry of Natural Resources, Hohai University, Nanjing, China

²Key Laboratory of Ministry of Education for Coastal Disaster and Protection, Hohai University, Nanjing, China

³College of Oceanography, Hohai University, Nanjing, China

⁴University of Northern British Columbia, Prince George, Canada

⁵Southern Marine Science and Engineering Guangdong Laboratory (Zhuhai), Zhuhai, China

⁶Department of Physics, Imperial College London, London, UK

⁷Atmospheric and Oceanic Sciences Program, Princeton University, Princeton, NJ, USA

Key Points:

- An objective definition of TC rapid intensification is developed by clustering the intensification rate, initial intensity, and size.
- A new threshold of 45 kt/24h (23.2 m/s/24h), higher than the widely-used 30 kt/24h (15.4 m/s/24h), is determined for the ocean globally.
- The thresholds for all basins are the same as the global value except for the North Atlantic and East Pacific where they are 40 kt/24h.

Abstract

Rapid intensification (RI) of tropical cyclones (TCs) provides a great challenge in operational forecasting and contributes significantly to the development of major TCs. RI is commonly defined as an increase in the maximum sustained surface wind speed beyond a certain threshold within 24 h. The most widely used threshold is 30 kt (15.4 m/s), which was determined statistically. Here we propose a new definition for RI by objectively clustering TCs using the intensification rate, initial intensity, and radius of the maximum wind speed. A group of 770 samples is separated at a threshold of 45 kt (23.2 m/s). The threshold is 40 kt (20.6 m/s) for the western North Atlantic, where TC size measurements are more reliable. Monte Carlo experiments demonstrate that the proposed threshold is robust even considering the uncertainty in RMW of as high as 30 km. We show that, when a TC undergoes RI, its maximum wind speed is approximately 60 ± 15 kt (30.9 ± 7.7 m/s) and the radius of the maximum wind speed is 45 ± 20 km. The new threshold outperforms the conventional threshold of 30 kt/24h in (1) describing the bimodal distribution of lifetime maximum intensity, and (2) explaining the annual count of Category 5 TCs. This new definition provides a more physically-based threshold and describes a more reliable representation to the extreme events. Although more comparisons are needed for operational application, it is likely to be desirable for process-based case studies, and could provide a more valuable metric for TC intensification classification and research.

1 Introduction

Rapid intensification (RI) is the dramatic strengthening of a tropical cyclone (TC) over a short period and poses a challenge for short-term weather forecasting and TC simulation (Rappaport et al., 2012; Rogers et al., 2013; Kaplan et al., 2015; Cangialosi et al., 2020; DeMaria et al., 2021; L. Wu et al., 2022; Emanuel, 2017). RI also has a substantial influence on the climatological distribution of TC intensity and most intense TCs undergo RI during their lifetimes (Lee et al., 2016).

Thus, RI is undoubtedly important in understanding TCs. RI is commonly defined as an increase in the maximum sustained surface wind speed (V_{\max}) of at least a certain threshold within 24 h. The most widely used threshold was proposed by Kaplan and DeMaria (2003), who defined RI as the 95th percentile of over-water 24-h intensity changes in the Atlantic TCs, which was 30 kt/24h. However, many other thresholds exist in the

literature. For instance, Kaplan et al. (2010) discussed the thresholds of 25 (12.9 m/s), 30 (15.4 m/s) and 35 kt (18.0 m/s) per 24 h, and highlighted the practical importance of the RI threshold for operational forecasting. Lee et al. (2016) documented 35 kt/24h as the optimal RI threshold describing the bimodal distribution of the lifetime maximum intensity (LMI).

The above statistical thresholds are invaluable and have been widely used in analyses of both internal and environmental processes during RI. However, the conclusions depend heavily on the chosen threshold, and one may reasonably question whether thresholds can be defined by other ways rather than statistically. A more rigorous definition of RI is desirable, especially for process-based studies. Here we revised the conventional threshold via clustering intensification-related metrics, and thereby proposed a threshold considering some of physical properties of the vortex. The physical mechanisms underlying TC intensification are complex and much effort has been devoted to understanding them (Y. Wang & Wu, 2004; Montgomery & Smith, 2014; Emanuel, 2018). Environmental and inner-core processes may both play important roles in determining whether and when a TC will undergo RI. Here, we focus on the initial vortex state, represented by TC intensity and vortex size metrics, such as V_{\max} and the radii of gale-force (34-kt, R_{34}) and maximum winds (RMW). These metrics were selected because they are routinely reported by the operational centers and their effects on intensification have been demonstrated in both observational and theoretical studies.

A TC of medium intensity is more likely to undergo RI (Kaplan et al., 2010; Xu & Wang, 2018; Y. Wang et al., 2021). When a TC is relatively weak, the inner-core inertial stability and heating efficiency increase with intensity, and thus, the TC intensifies (Shapiro & Willoughby, 1982; Schubert & Hack, 1982). However, as the intensity of the storm nears its maximum potential intensity, the frictional dissipation counteracts the heating efficiency, and the intensification rate decreases. The maximum intensification rate is typically observed at approximately 60~70 kt, where the intensification potential is close to the weakening rate due to surface friction (Kaplan et al., 2010; Y. Wang et al., 2021).

In addition, the vortex size reflects feedback between the primary circulation and inner-core processes (Mallen et al., 2005), and affects the subsequent intensification (Emanuel, 1989). Studies based on best-track data have confirmed that RI events rarely occur when

RMW is larger than 100 km, because a small RMW favors intensification due to the conservation of angular momentum (Carrasco et al., 2014; Xu & Wang, 2018). It has also been known that the inward contraction of eye-wall, usually represented by a decrease in RMW, often occurs simultaneously with intensification (Shapiro & Willoughby, 1982; Schubert & Hack, 1982). In a seminal study, Shapiro and Willoughby (1982) showed that the response of low-level tangential wind tendency to diabatic heating is greater inside RMW than outside. Thus, when RMW decreases, the potential energy of the vortex increases and the balanced tangential winds intensify simultaneously. Recent studies also show that rapid contraction of RMW could occur prior to RI (Stern et al., 2015; Li et al., 2019, 2021; Li, Wang, & Tan, 2022; Q. Wu & Ruan, 2021). However, cases also exist in which RI co-occurs with steady RMW (Kieu, 2012; Qin et al., 2018). Therefore, we only considered RMW instead of its changes in this work.

Other metrics that reflect the outer size of the TC, specifically the average radius of the 34-kt wind speed (R_{34}) and TC fullness, were also examined in this study. Notably, Carrasco et al. (2014) showed that R_{34} aids in RI prediction. In addition, Guo and Tan (2017) proposed the concept of TC fullness, a metric calculated from RMW and R_{34} [defined as $(1 - \frac{RMW}{R_{34}})$], and demonstrated that a high TC fullness is essential for intense TC development. In this study, a joint clustering method was implemented based on the K-means algorithm. Such clustering algorithms have been widely used in TC research. For instance, Camargo et al. (2007) utilized joint clustering analysis to group western North Pacific TC tracks based on their locations of genesis and subsequent tracks. Arnott et al. (2004) analyzed the characteristics of extra-tropical transitions based on the results of K-means. Guo and Tan (2017) clustered the evolution curves of the Atlantic Hurricanes to analyze TC fullness. Moreover, clustering has been widely used to detect outliers or extreme events (e.g., Chawla & Gionis, 2013). Therefore, we chose to detect extreme intensification using this technique. Using a joint clustering algorithm, the common features for the RI events were extracted and the RI and non-RI clusters were subsequently separated. We focused on Atlantic TCs to the west of 55°W from 2004 to 2020, mainly considering better data quality than those for other basins and periods. Our data pre-processing and main methods, including the unsupervised clustering technique, are introduced in Section 2. The sensitivity experiments and statistical characteristics of TCs undergoing RI, as defined with the new threshold, are presented in Sec-

tion 3, where the performance of this new threshold is also explored. Section 4 discusses the main results and summarizes the key findings.

2 Data and Methods

TC data were obtained from the International Best Track Archive for Climate Stewardship (IBTrACS, v4r00, Knapp et al., 2010). For consistency and quality, we only utilized data from the National Hurricane Center for the Atlantic and East Pacific, and from the Joint Typhoon Warning Center for the remainder of the globe, for 2004–2020. The two USA agencies measure intensity as the 1-min sustained maximum 10-m wind speed (V_{\max}). The intensification rate was defined as the change of V_{\max} during each 24-h interval (hereafter ΔV_{24}). We only obtained records for the standard observational times: 00, 06, 12, and 18 Coordinated Universal Time (UTC). RI may occur for consecutive 24-h periods and some of the tracks overlapped. In our study, we only selected TCs between 30°N and 30°S to minimize the influence of extra-tropical transition. To eliminate the topographic effects, we chose only TC tracks over the ocean, and all TC centers were at least 100 km from the coastline. The distance to the nearest landmass was provided by IBTrACS for each TC location. This pre-processing is similar to previous studies (e.g., Kaplan & DeMaria, 2003; Ma et al., 2019).

Environmental factors were also analyzed, with the relative humidity, wind, and sea surface temperature (SST) data obtained from the fifth generation of atmospheric reanalysis from the fifth version of ECMWF re-analysis (ERA5, Hersbach et al., 2020). The horizontal and temporal resolutions of the ERA5 data are 0.25° and 6 hours, respectively. For ERA5 we also analyzed the data for 00, 06, 12, and 18 only.

Since 2004, the wide use of satellite, in situ observations, aircraft reconnaissance and routine post-season analyses have significantly reduced the observation error, especially for the Atlantic basin to the west of 55°W. Unfortunately, large uncertainties still exist in the RMW data. Even for western North Atlantic, RMW was not best tracked until the 2021 hurricane season (Landsea, 2022), although the data during earlier periods has been utilized extensively for various basins (e.g., Xu & Wang, 2015, 2018; Q. Wu & Ruan, 2021; Li, Wang, & Tan, 2022). Thus an independent test was performed, by applying the best-tracked data of 2021 to the clustering model that was trained with the data from 2004 to 2020. Landsea (2022) also reported that the uncertainty with RMW

observation can be as high as 16 nautical miles (30 km) for TCs stronger than 64kt (Category 1). As in Li, Tang, and Wang (2022), we carried out Monte Carlo experiments here to estimate the potential influence of observation uncertainties, in which 1,000 samples were produced by adding random noise from a Gaussian distribution with a mean of 0 and a standard deviation of 30 km to each RMW value. In addition, to estimate the influence of uncertainty from V_{\max} measurements, we conducted another Monte Carlo experiment, in which 1,000 subsamples were produced by adding random noise from a uniform distribution on the interval ± 10 knots to each intensity change value (Bhatia et al., 2019).

The clustering algorithm requires input samples, which consisted of a combination of the initial V_{\max} and/or initial TC size metrics (RMW, R_{34} , TC fullness) at $t = 0$ h, and the ΔV_{24} of the subsequent 24-h period. The primary clustering algorithm used in this study was K-means. This algorithm partitions the samples into subsets while minimizing the variance within each cluster. In addition, another unsupervised artificial neural network, the self-organizing map (SOM) (Kohonen, 1990, 2013; Liu et al., 2006) was used for comparison. The SOM fits initially random weights to observations by comparing their Euclidean distances through competitive training. For both methods, the number of clusters, K , significantly affects the clustering results; their performance can be evaluated using the silhouette (Rousseeuw, 1987) and Davies-Bouldin scores (Davies & Bouldin, 1979). The silhouette score measures the similarity of the points within each cluster and is defined as follows:

$$S = \frac{b - a}{\max(a, b)}, \quad (1)$$

where a is the mean distance between one point and all other points in the same cluster and b is that for the nearest cluster. Thus a higher silhouette score indicates higher similarity within each cluster and a better clustering model. In contrast, the Davies-Bouldin score compares the average similarity between each pair of clusters. It can be defined as follows:

$$DB = \frac{1}{k} \sum_{i=1}^k \max_{i \neq j} R_{ij}, \quad (2)$$

where R_{ij} measures the ratio between cluster diameter (s_i , i.e., the average distance between cluster centroid and the points within the cluster C_i) and the distance between the currents C_i and C_j . Therefore, a smaller Davies-Bouldin score indicates a better clustering result. Both metrics were used in this study to calculate the distance of clusters in the parameter space and determine the optimal K .

The V_{\max} , RMW, R_{34} and TC fullness data were used for clustering. The environmental factors were not analyzed for clustering because only the properties of the initial vortex were considered in this study. The intensity and size data were pre-processed and normalized before input to the clustering models, because their units and scales are different. All the variables are available for each input sample. It should be noted that we only consider the intensifying events for clustering due to their practical importance. Seven sensitivity experiments were performed to find the optimal combination of input variables, and the main model we used here clustered the input of V_{\max} , RMW and ΔV_{24} into 8 clusters. The details of these experiments are summarized in the supplementary material (Text S1 and Table S1).

3 Results

3.1 Overall distribution of the intensification rate

A total of 886 storms and 12530 intensifying events were extracted from the global best-track data, and 107 storms and 1443 events for the western North Atlantic basin. The probabilistic distribution (Fig. 1A) of ΔV_{24} for the global basins is continuous and no discernible gap appears near 30 kt/24h, which is the traditional threshold. Moreover, this continuity suggests that the traditional threshold, which only considers the intensification rate, is a purely statistical or practical choice. This is similar to the findings of Kowch and Emanuel (2015). Fig. 1B depicts the cumulative frequency distribution, similar to that in Fig. 2 of Kaplan and DeMaria (2003), but using our data for all TCs instead of the North Atlantic alone. However, the curves for the different initial intensities did not converge until ΔV_{24} was above the 97th percentile (approximately 40 kt/24h). This discrepancy partially justifies the need for further examination of the statistical RI thresholds.

Intensification is likely strongly influenced by initial state of the vortex, which are reflected in part by the initial intensity and size. Thus, it is useful to analyze the joint

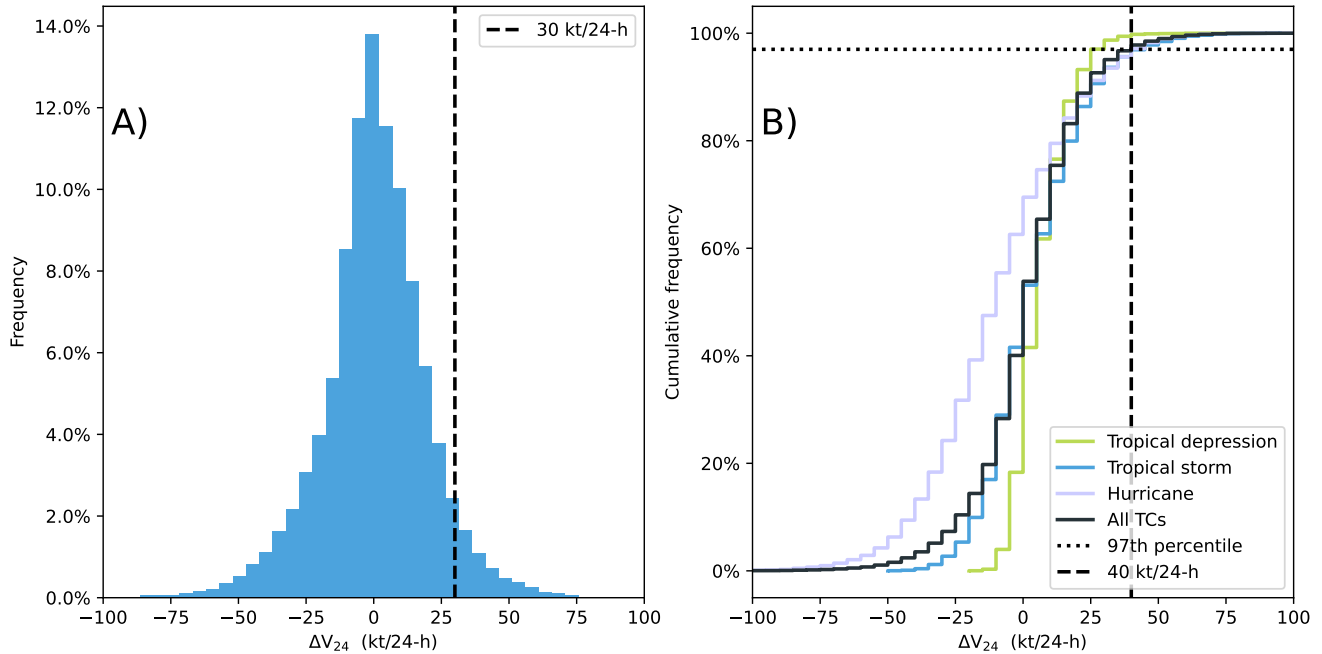


Figure 1. (A) The frequency distributions of 24-h intensification rate (ΔV_{24}); (B) The cumulative frequency distributions of ΔV_{24} for the initial intensity of different scales, i.e., Tropical depressions ($V_{\max} \leq 33$ kt), Tropical storms ($34 \leq V_{\max} \leq 63$ kt) and Hurricanes ($V_{\max} \geq 64$ kt). Note the distributions in this figure were calculated using all ΔV_{24} instead of the positive values alone.

frequency distributions of ΔV_{24} and the initial V_{\max} and RMW (Fig. 2). The ΔV_{24} increased with V_{\max} when V_{\max} was lower than approximately 60 kt (30.9 m/s), and ΔV_{24} could be up to 100 kt/24h. When the TC was stronger than 75 kt (38.6 m/s), ΔV_{24} decreased. TCs with this intensity range are generally well organized and far from their maximum potential intensity (Kaplan et al., 2010; Y. Wang et al., 2021). Additionally, RI was also more likely to arise when RMW is less than 100 km, and ΔV_{24} generally decreased as the RMW increased. A smaller RMW reflects higher inner-core inertial stability and dynamic efficiency, which enhances intensification (Schubert & Hack, 1982). The 95th percentile of ΔV_{24} is also significantly higher in this range of RMW and V_{\max} . For the North Atlantic, where the TC size measurement is more reliable, ΔV_{24} was generally lower; however, the V_{\max} and RMW trends were similar. ΔV_{24} increased with V_{\max} at values of less than approximately 60 kt, and decreased with V_{\max} at values of higher

than 80 kt. RI generally occurred when RMW was smaller than 100 km. These results align with the findings from previous studies (Carrasco et al., 2014; Xu et al., 2016; Xu & Wang, 2018). In addition, RI mainly occurs with medium V_{\max} and small RMW, which improves the separation of RI events in parameter space and promotes clustering performance.

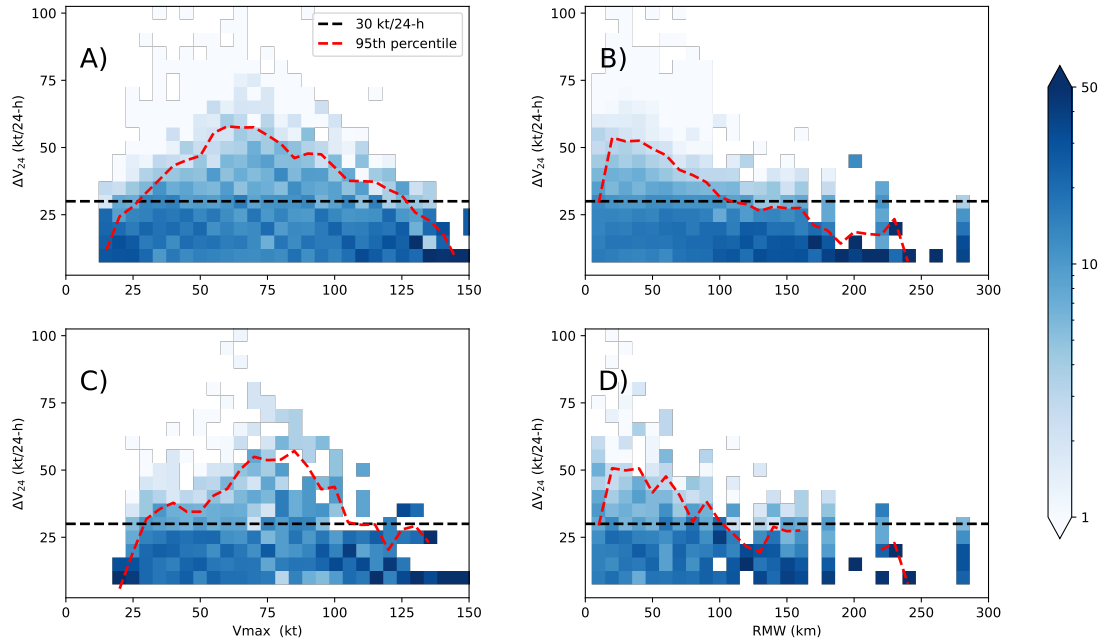


Figure 2. The ratio of positive ΔV_{24} as a function of (A) the initial maximum sustained surface wind speed (V_{\max}) and (B) the initial radius of the maximum wind (RMW) for the global basins. (C) and (D) are the same as (A) and (B) but for the western North Atlantic basin. The y-axis in each subplot is ΔV_{24} (units: kt/24h) and the x-axis shows the initial V_{\max} (units: kt) and RMW (units: km), respectively. The unit for the blue shadings is %.

3.2 Sensitivity experiments

We performed a series of sensitivity experiments to choose an optimal number of clusters (K) and combination of input variables. The best performance is found in the model with initial V_{\max} , RMW and ΔV_{24} as input, which is shown here as an example. When the intensifying events were clustered into 8 groups, the Davies-Bouldin score reached

a minimum, and the silhouette score was relatively high (Fig. 3). These metrics indicated the distance between clusters reaches the minimum in the three-dimensional space (V_{\max} , RMW and ΔV_{24}) when clustered into 8 groups. We then analyzed ΔV_{24} with such a configuration, and an 'RI' cluster with a significantly higher ΔV_{24} was distinctly separated from the remainder of the dataset (Fig. 4A). The minimum ΔV_{24} of this 'RI' cluster is 45 kt/24h. Fig. 3 suggests that clustering the TCs into six groups was also reasonable. However, the overlaps between the RI and non-RI clusters were much broader, although RI clusters still emerged at a threshold of approximately 35-40 kt/24h (Fig. 4B). Therefore, the 8-cluster model was chosen owing to its superior overall performance. Most of the 770 TC events in the RI cluster had a ΔV_{24} greater than or equal to 45 kt/24h. For North Atlantic, on the other hand, a similar optimal configuration was also found, and the threshold is 40 kt/24h for North Atlantic. The detailed results of other sensitivity experiments can be found in the supplementary text.

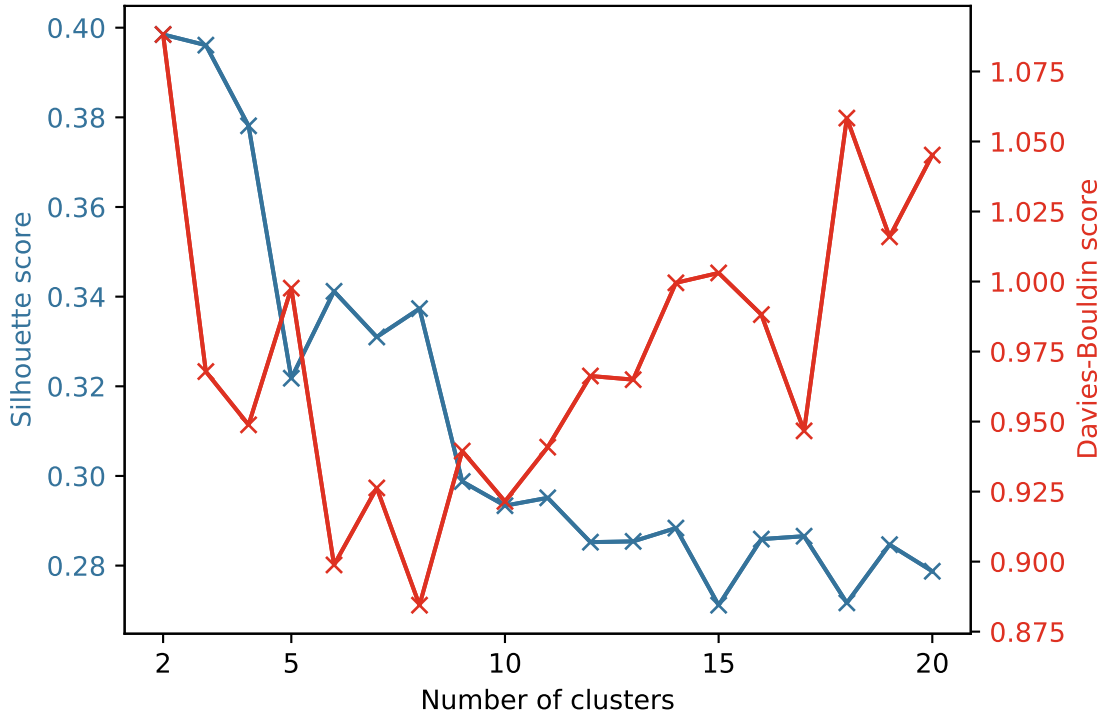


Figure 3. The silhouette and Davies-Bouldin scores as functions of the number of clusters when initial V_{\max} , RMW and ΔV_{24} are input for clustering. The models were trained using global data.

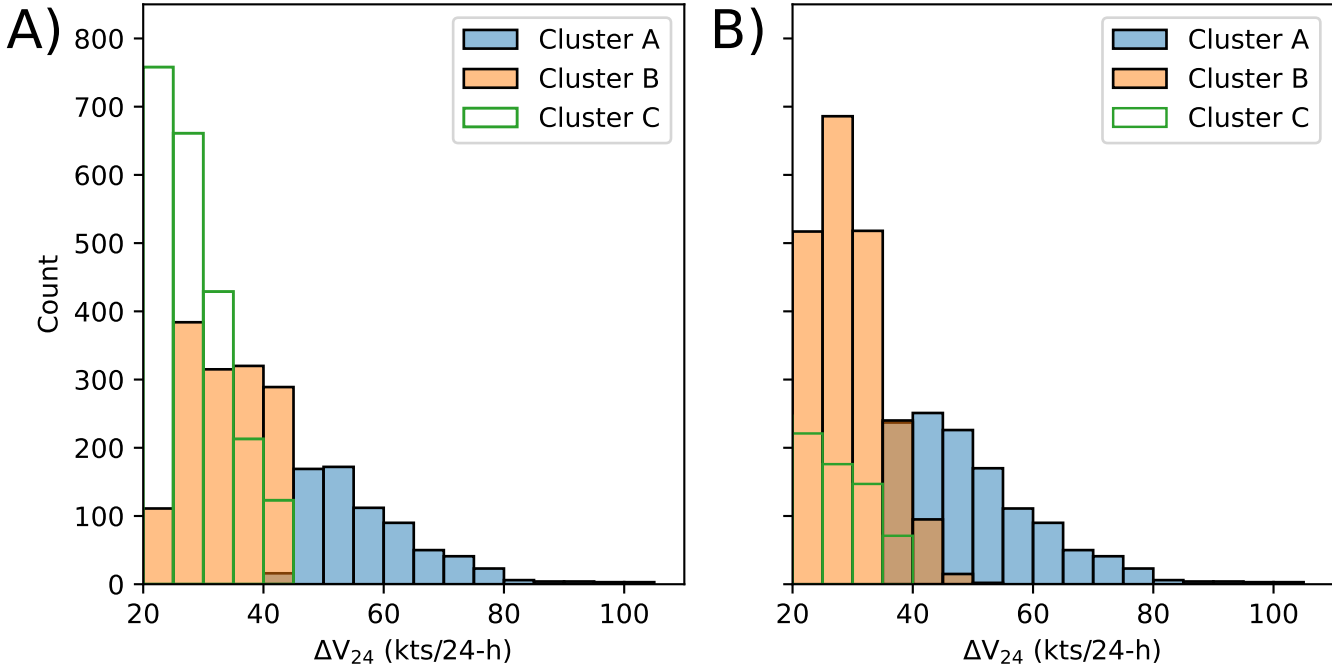


Figure 4. Intensification rate (ΔV_{24}) of different clusters with (A) eight and (B) six clusters when initial V_{\max} , RMW and ΔV_{24} are input for clustering. The rapid intensification (RI) cluster is labeled as Cluster A in both subplots. The models were trained using global data. Only the three most rapidly intensifying clusters are plotted for better display clarity. The results with all clusters can be found in Fig. S1.

The robustness of clustering highly depends on the quality of best-track data, especially considering the uncertainty with RMW is high. In the Monte Carlo experiments, we found the threshold of 45 kt/24h is robust even when the uncertainty of RMW was set to 30 km. In the 1,000 perturbed samples, 95% (952) achieved the same threshold of 45 kt/24h while 5% (48) produced a threshold of 40 kt/24h. In addition, when the North Atlantic model was applied to the 2021 hurricane season, an RI group was also classified and the minimum ΔV_{24} (i.e., threshold) was 40 kt/24h (Fig. 5), consistent with the threshold identified using data of earlier periods. The results of above two tests indicate the proposed threshold is robust, even considering the high uncertainty of RMW measurements. Nevertheless, the threshold of 30 or 35 kt/24h was not found in these experiments.

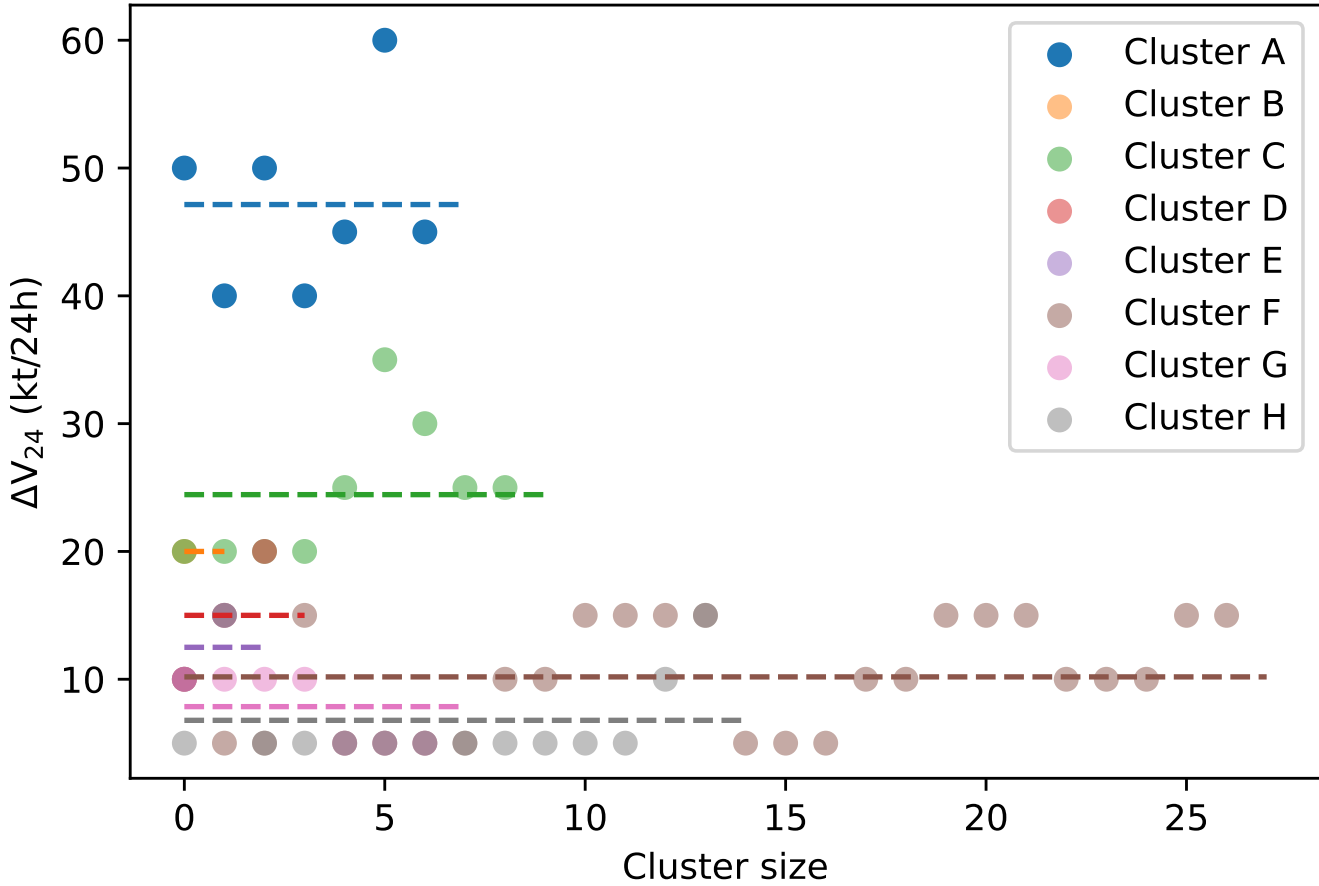


Figure 5. Intensification rate (ΔV_{24}) of different clusters for the 2021 North Atlantic hurricane season. The rapid intensification (RI) cluster is labeled as Cluster A. The dashed lines depict the average ΔV_{24} for each cluster.

3.3 Characteristics and evaluation of the new threshold

The threshold of 45 kt/24h was selected due to its better overall performance in the sensitivity experiments. This threshold corresponds to the 97th percentile of the global over-water ΔV_{24} . For the global basins, the mean ΔV_{24} , V_{\max} and RMW of this cluster were 54 kt/24h, 62 kt and 45 km, respectively (Table 1). On the other hand, these properties for the TCs with a ΔV_{24} of over 30 kt/24h, were 40 kt/24h, 58 kt and 52 km, respectively.

Analyses for the individual basins were performed next. The global RI threshold of 45 kt/24h was found for most basins, except for the North Atlantic (NA) and East Pacific (EP), where the RI threshold was 40 kt/24h (Table 1). These differences are likely to be an artifact since the measurements were provided by varied agencies. However, it is also possible that the background ΔV_{24} varies among basins (Fig. 6), as already noticed by previous studies (e.g., Xu & Wang, 2015, 2018). For instance, The intensification rates are significantly higher in western North Pacific (WP) and North Indian Ocean (NI) than in EP and NA. The 95th percentile of ΔV_{24} in the former two basins was 40 and 40 kt/24h, respectively, while in the latter two basins it was 35 kt/24h. Monte Carlo experiments also showed that the 95th percentile of ΔV_{24} in EP and NA is 37.5 kt/24h, while for the other basins it is 41.5 kt/24h. Therefore different thresholds exist even the percentile-based method was used. Such differences can be attributed to various environmental conditions. Using an idealized numerical simulation, Li et al. (2021) noted a higher ΔV_{24} with a vertical sounding from WP than NA, especially when SST is lower than 28°C.

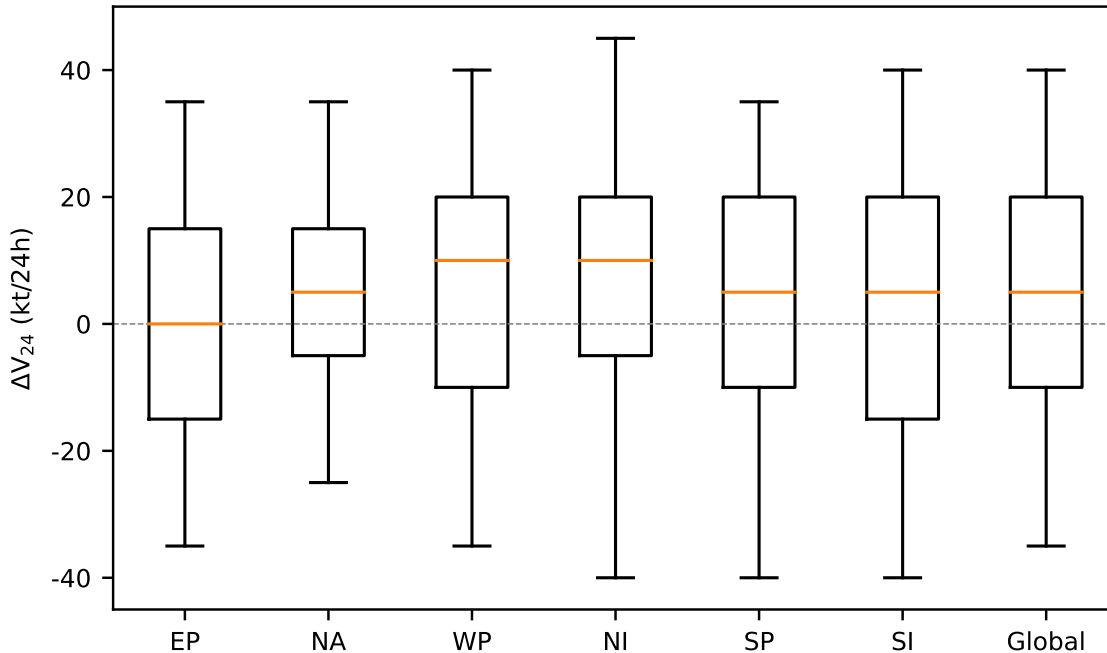


Figure 6. Boxplot of background ΔV_{24} for different basins. The lower and upper ends of the box show the 25th and 75th percentiles, the middle line shows the 50th percentile, and the whiskers show the 5th and 95th percentiles, respectively.

Table 1. The RI thresholds, their corresponding percentile rank among the samples, and the mean and standard deviation of ΔV_{24} , V_{\max} and RMW of the RI clusters for the global and individual basins. (NATL, North Atlantic; EPAC, East Pacific; WPAC, Western North Pacific; SPAC, South Pacific; NIO, North Indian Ocean; SIO, South Indian Ocean). Note the percentiles were calculated using all ΔV_{24} instead of the positive values alone.

	RI threshold (kt/24h)	Percentile	ΔV_{24} (kt/24h)	V_{\max} (kt)	RMW (km)
Global	45	97 th	53.7 ± 9.8	61.7 ± 16.6	46 ± 20
NATL	40	98 th	49.4 ± 11.0	64.3 ± 14.4	41 ± 23
EPAC	40	96 th	51.8 ± 9.9	59.9 ± 14.7	46 ± 19
WPAC	45	97 th	55.7 ± 9.0	63.8 ± 15.7	44 ± 17
SPAC	45	96 th	55.3 ± 9.1	59.6 ± 15.6	51 ± 21
NIO	45	96 th	60.4 ± 10.0	56.5 ± 8.8	47 ± 19
SIO	45	97 th	55.0 ± 10.1	49.6 ± 11.3	53 ± 12

Over all RI clusters, the initial intensity was approximately 60 ± 15 kt, and the radius was approximately 45 ± 20 km, while RMW was significantly larger (65 ± 37 km) for the non-RI clusters (Table S2). Moreover, intensity and size varied significantly among many basins. For instance, the average ΔV_{24} of the RI cluster for the North Indian Ocean (60.4 kt/24h) was significantly higher than that for the North Atlantic (49.4 kt/24h). The RI cases over the South Indian Ocean were initially significantly weaker and larger than those over the western North Pacific, whereas the typical ΔV_{24} and RI thresholds were similar for the two basins. Using a single threshold of 30 kt/24h failed to detect many of these differences. For example, a significant differences in RMW and initial intensity were observed between the RI events detected by clustering over the North Indian Ocean and western North Pacific. However, when the conventional threshold was used, there was no such difference in the inner-core size. Significant difference ($p < 0.01$) also exists in ΔV_{24} between Western and Eastern Pacific basins, as determined by the new threshold, while no difference could be detected ($p = 0.7$) using the conventional threshold of 30 kt/24h. However, we used a fixed period of 24h for all RI events and some of the events overlapped, and the results are likely to be different if consecutive RI events are considered as one.

The performance of the new threshold in explaining the distribution and variation of TC intensity was also examined. Lee et al. (2016) noted that the lifetime maximum intensity (LMI) follows a bimodal distribution, and the modes indicate two types of TCs: those that undergo RI (RI TCs) and those that do not (non-RI TCs). Here, we compared the effects of different thresholds on the distributions of the global and North Atlantic TCs (Fig. 7). Note only the TC data with both V_{\max} and RMW recordings over the period 2004–2020 were used and thus the distributions differ slightly from Lee et al. (2016), who used all data from 1981–2012. Similar to their results, RI TCs, defined with either the clustering or traditional threshold, comprised the majority of the major TCs ($LMI \geq 96$ kt, Category 3), with a peak at approximately 120 kt. However, the clustering threshold was more effective in separating the non-RI TCs, especially for the North Atlantic. When the clustering threshold was used, 80% of RI TCs had an LMI of over 96 kt for the North Atlantic, and this ratio is 82% for the global TCs. In contrast, with the threshold of 30 kt/24h, 65% and 72% of the RI TCs became major TCs for the North Atlantic and the globe, respectively.

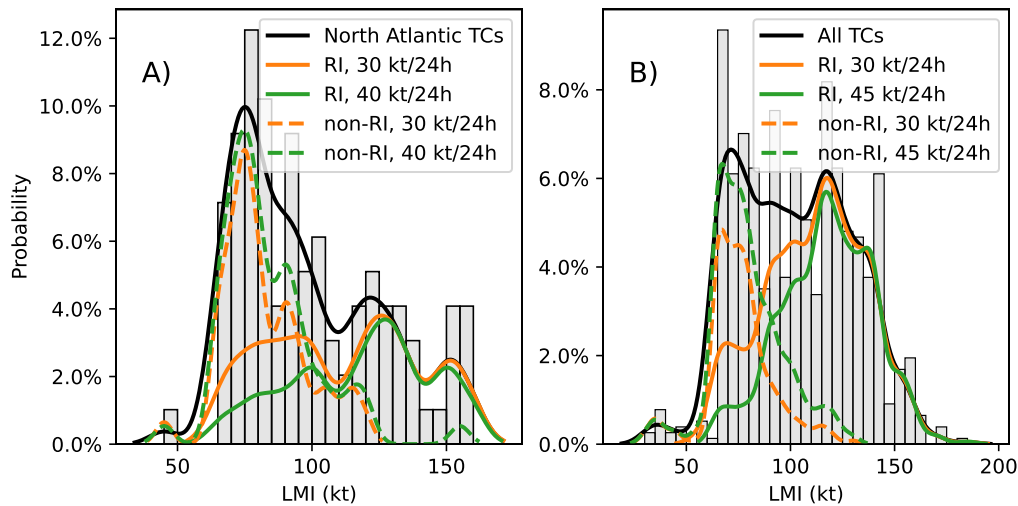


Figure 7. Distributions of LMI for (A) the western North Atlantic and (B) the global TCs. Probability Distribution Functions (PDFs) were calculated using 2004–2020 tropical cyclone LMI. The grey histograms and black line depict the distribution of all TCs. The orange and green lines show the PDFs for the TCs that underwent RI defined with by clustering (40 kt/24h for the North Atlantic and 45 kt/24h for the global TCs) and traditional thresholds (30 kt/24h), respectively. The PDFs were smoothed using kernel density estimation with a bandwidth of 0.2.

The high correlation between the number of RI events and major TCs further demonstrated the benefits of the new threshold. Fig. 8 plots the LMI against the number of RI events with the traditional and the proposed thresholds. When the clustering threshold was used, LMI clearly increased with the number of RI events per storm. However, when the threshold of 30 kt/24h was used, the number of RI events was not highly related to LMI, especially for the Category 5 TCs ($LMI \geq 137$ kt). This was also demonstrated by a higher correlation between LMI and the number of RI events (0.62 vs 0.52, $p < 0.05$). In addition, the number of RI events identified by the new threshold better explained the annual variation of the major TCs (Fig. 8C), especially for Category 5 TCs, as indicated by relatively larger slopes of their fitted lines. The correlations between the number of TCs stronger than Category 3 ($LMI \geq 96$ kt) and the clustering-based and conventional thresholds were both 0.81. However, the correlation between the number of Category 5 TCs and RI events with the new threshold was 10% higher than that with the traditional one (0.85 vs 0.75, $p < 0.05$). These improvements demonstrated the potential of the proposed threshold in the research of major TCs.

We further analyzed the environmental factors affecting the intensification processes in the western North Atlantic, namely mid-level relative humidity, deep vertical wind shear, and SST (Fig. 9). These variables were similar between the RI events, as defined by the clustering and traditional thresholds. Although a slightly higher mid-level humidity, lower vertical wind shear, and higher SST were observed for RI events defined by the clustering threshold, the differences are not statistically significant. The results partially validate our choice of using metrics representing the initial vortex property only.

4 Discussion and conclusion

Rapid intensification of great importance in TC research. Conventionally, RI is defined statistically. In this study, we proposed a physically orientated threshold and incorporated properties of the vortex into its definition. To do so, we treated RI as an extreme-detecting problem and cluster the initial V_{\max} and RMW, with a subsequent ΔV_{24} for all global TCs from 2004 to 2020. These variables were selected because they define the initial state of the vortex before RI, as demonstrated by previous theoretical and observational studies (e.g., Y. Wang et al., 2021; Li et al., 2021; Mallen et al., 2005; Carrasco et al., 2014) and our sensitivity experiments. Over 12000 events extracted from the IB-TrACS best-track data were clustered using the K-Means clustering algorithm; one clus-

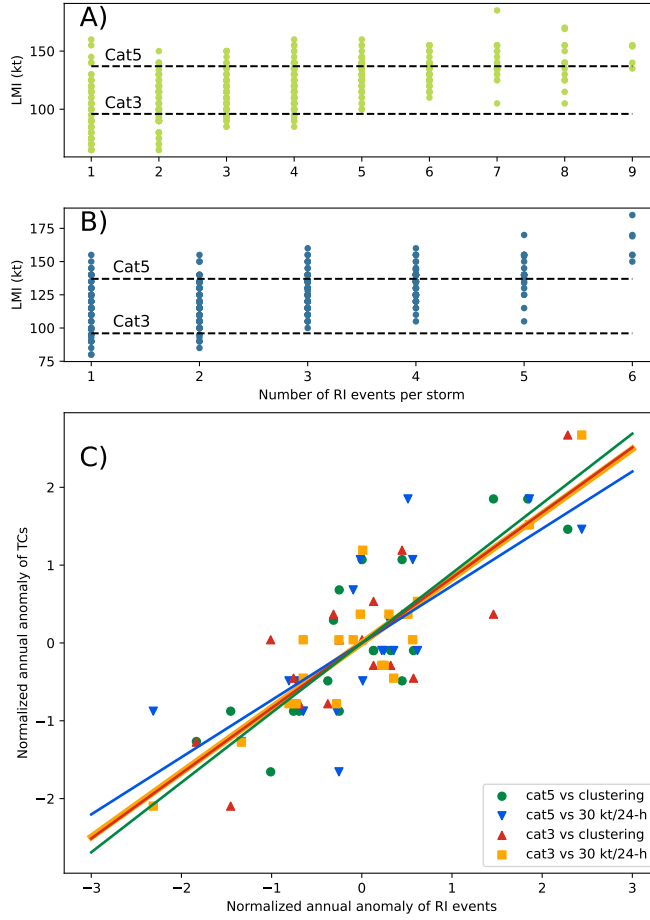


Figure 8. The distribution of LMI and the number of RI events per storm with (A) the threshold of 30 kt/24-h and (B) the clustering threshold. (C) Scatter plot of the normalized annual number of RI events versus the normalized annual number of TCs of different categories. Each variable was normalized using its own mean and standard deviation prior to plotting. The solid lines show the linear regression.

ter with a minimum ΔV_{24} of 45 kt/24h (23.2 m/s/24h) was thereby distinctly separated from the others. A significant gap between the RI and non-RI clusters was found, indicating that RI can be separated statistically and physically by vortex property. The RI

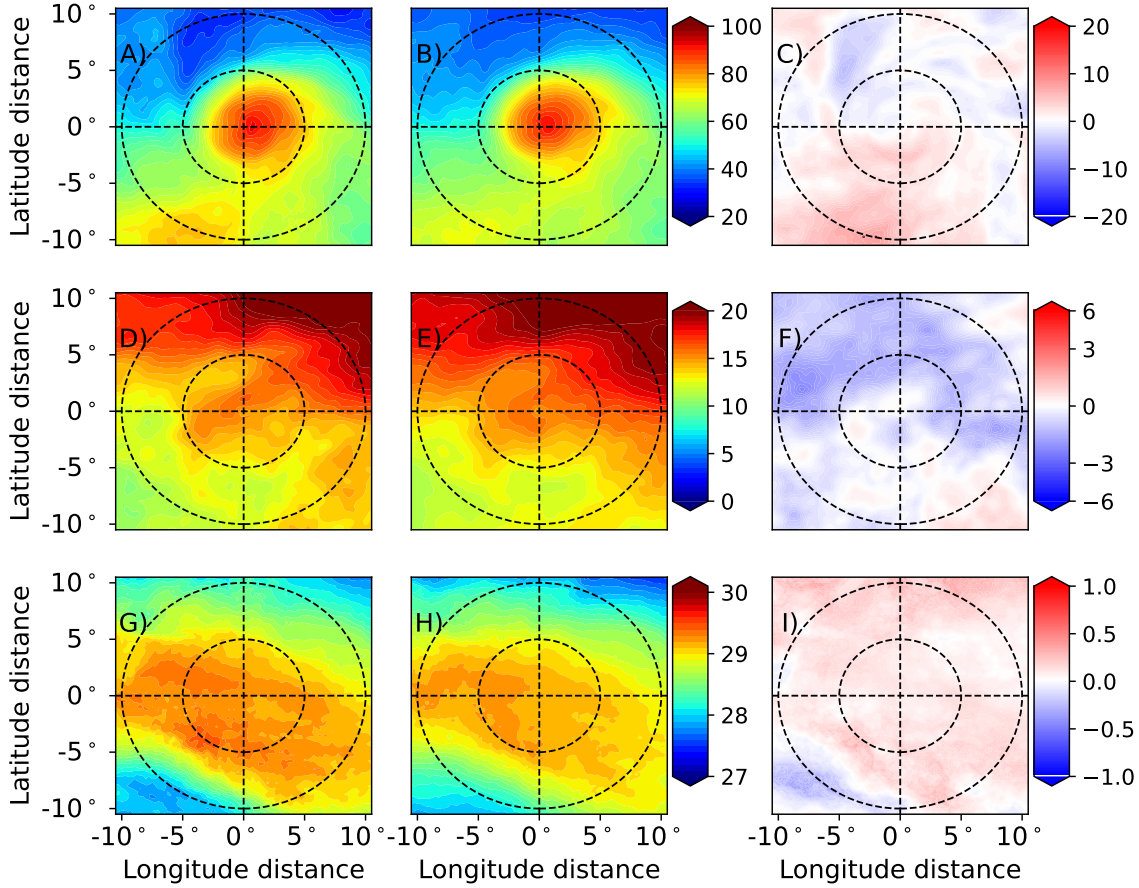


Figure 9. Composite fields of: (A), (B), (C) 600-hPa relative humidity (units: %; shaded); (D), (E), (F) 200- and 850-hPa vertical wind shear (units: m/s); and (G), (H), (I) sea surface temperature (units: °C) for the (A), (D), (G) RI using the clustering threshold (≥ 40 kt/24h); (B), (E), (H) RI using the traditional threshold (≥ 30 kt/24h); and (C), (F), (I) the difference. The units for the x- and y-axes are degrees. The 2 circles indicate radii of 5 and 10 degrees from the TC center.

threshold was the same as the global value across all the individual basins except for the North Atlantic and East Pacific, where it was 40 kt/24h (20.6 m/s/24h).

It should be noted that the results obtained from the clustering analysis rely heavily on data quality. RMW has a relatively large uncertainty because of limited temporal and spatial resolution in the satellite observations (Demuth et al., 2004), although the data has been widely used for various basins (e.g., Carrasco et al., 2014; Xu & Wang, 2018, 2015; Q. Wu & Ruan, 2021; Li, Wang, & Tan, 2022). Even for the Atlantic basin, where we have high confidence on the data quality, the uncertainty could be as high as

16 nm (30km) (Landsea, 2022). To assess the impact of data uncertainty, we conducted Monte Carlo experiments and an independent test for the 2021 hurricane season. The results demonstrated the robustness of the proposed threshold, even with an uncertainty of 30 km in RMW. Nevertheless, this uncertainty is expected to decrease with improved observation facilities (e.g., Combot et al., 2020) and the clustering results could be revised with more accurate measurements, especially for the basins other than the Atlantic.

We do not compare performances of the two thresholds in operations due to the scope of this work. The operational and practical choices of RI definition could be based purely on frequency. However, a more rigorous definition based on, for instance, the initial vortex state as advocated here may be desirable for case-based process study and trend analysis. As a first step, we present this new definition of RI from a different angle and emphasize on physical properties of the vortex behind the results. The clustering method identified an initial wind speed of 60 ± 15 kt and an RMW of 45 ± 20 km as the typical conditions for the RI cluster. While for the non-RI clusters, the average RMW mounts up to 65km. Around these initial values, eye and eye-wall formation would be expected (Vigh et al., 2012). The onset wind speed cannot be much larger because, above this value, the frictional dissipation increases and ΔV_{24} is constrained as the TC approaches the maximum potential intensity (Y. Wang et al., 2021). On the other hand, a small RMW reflects a high inner-core inertial stability and dynamical efficiency, which enhances intensification (Schubert & Hack, 1982). The inertial stability within the RMW was on the order of 10^{-3} s^{-1} or about 20 f at 20 °N and became important near these wind speeds. A small RMW also favors intensification due to the conservation of angular momentum. Both numerical and observational studies (Li et al., 2021; Li, Wang, & Tan, 2022; Y.-F. Wang & Tan, 2020; Sitkowski et al., 2011; Fischer et al., 2020) showed the typical RMW value during RI is approximately 30 to 50 km, which is consistent with our results. These results also suggest that accurate measurement and prediction of RMW near V_{\max} of 60 kt would be expected to play a significant role in improving RI predictions.

Moreover, an advantage of the clustering threshold is its ability to explain the bimodal distribution of the LMI. Both clustering and traditional thresholds can explain the secondary peak at around 120 kt. However, Lee et al. (2016) reported that in the North Atlantic, 30% RI TCs became minor TCs ($\text{LMI} < 96$ kt). The ratio reduced to 20% if the clustering threshold is used. Similar results were found for the global distribution. In addition, the new definition also showed a better correlation with the variation in the

annual number of Category 5 TCs over the past decades compared to that of the traditional threshold, demonstrating the potential and importance of this new threshold for major TC research.

Environmental factors are undoubtedly important for TC intensification and many of such factors are included in the forecasting systems (e.g., Kaplan & DeMaria, 2003). However, previous studies found that the environmental conditions for the RI and intensifying TCs are similar (Hendricks et al., 2010), and argued RI is a weak function of the environmental conditions (Kowch & Emanuel, 2015). We also found that the difference of the mid-level humidity, vertical wind shear and SST between the RI events, with different thresholds, is marginal. Therefore favorable environmental factors are essential, but are likely insufficient for RI. Although the environmental influences require further investigation, such results validate our selection of using the inner-core metrics only.

This work suggests the potential of clustering to define an RI threshold with an objective and plausible physical basis and demonstrates its advantages in explaining the distribution of major TCs. We did not directly compare the operational applications of proposed and conventional thresholds, but the higher threshold proposed here would reduce the sample size of RI events, which may impact its operational usefulness in some aspects. Systematic analyses are thus required, including the ability of operational systems in detecting RI events, influences of different precursors, and damage caused by different RI events, before the proposed threshold is used in operation.

Acknowledgments

This study is sponsored by the National Natural Science Foundation of China (42006036, 42130409), National Key Research and Development Program (2017YFA0604202), Fundamental Research Funds for the Central Universities (B210202141) and Natural Environment Research Council/UKRI (NE/V017756/1).

Open Research

The data used in this study is the International Best Track Archive for Climate Stewardship (IBTrACS) Version 4 (v4r00) and publicly available at <https://www.ncdc.noaa.gov/ibtracs/index.php?name=ib-v4-access>. ERA5 data is downloaded from <https://cds.climate.copernicus.eu/#!/home>.

References

- Arnott, J. M., Evans, J. L., & Chiaromonte, F. (2004, December). Characterization of Extratropical Transition Using Cluster Analysis. *Monthly Weather Review*, *132*(12), 2916–2937. Retrieved 2022-05-16, from <http://journals.ametsoc.org/doi/10.1175/MWR2836.1> doi: 10.1175/MWR2836.1
- Bhatia, K. T., Vecchi, G. A., Knutson, T. R., Murakami, H., Kossin, J., Dixon, K. W., & Whitlock, C. E. (2019, December). Recent increases in tropical cyclone intensification rates. *Nature Communications*, *10*(1), 635. Retrieved 2022-03-19, from <http://www.nature.com/articles/s41467-019-08471-z> doi: 10.1038/s41467-019-08471-z
- Camargo, S. J., Robertson, A. W., Gaffney, S. J., Smyth, P., & Ghil, M. (2007, July). Cluster Analysis of Typhoon Tracks. Part II: Large-Scale Circulation and ENSO. *Journal of Climate*, *20*(14), 3654–3676. Retrieved 2022-05-01, from <http://journals.ametsoc.org/doi/10.1175/JCLI4203.1> doi: 10.1175/JCLI4203.1
- Cangialosi, J. P., Blake, E., DeMaria, M., Penny, A., Latta, A., Rappaport, E., & Tallapragada, V. (2020, October). Recent Progress in Tropical Cyclone Intensity Forecasting at the National Hurricane Center. *Weather and Forecasting*, *35*(5), 1913–1922. Retrieved 2022-04-16, from <https://journals.ametsoc.org/doi/10.1175/WAF-D-20-0059.1> doi: 10.1175/WAF-D-20-0059.1
- Carrasco, C. A., Landsea, C. W., & Lin, Y.-L. (2014, June). The Influence of Tropical Cyclone Size on Its Intensification. *Weather and Forecasting*, *29*(3), 582–590. Retrieved 2022-07-06, from <https://journals.ametsoc.org/doi/10.1175/WAF-D-13-00092.1> doi: 10.1175/WAF-D-13-00092.1
- Chawla, S., & Gionis, A. (2013, May). k -means–: A unified approach to clustering and outlier detection. In *Proceedings of the 2013 SIAM International Conference on Data Mining* (pp. 189–197). Society for Industrial and Applied Mathematics. Retrieved 2022-07-06, from <https://epubs.siam.org/doi/10.1137/1.9781611972832.21> doi: 10.1137/1.9781611972832.21
- Combrot, C., Mouche, A., Knaff, J., Zhao, Y., Zhao, Y., Vinour, L., ... Chapron, B. (2020, November). Extensive High-Resolution Synthetic Aperture Radar (SAR) Data Analysis of Tropical Cyclones: Comparisons with SFMR Flights

- and Best Track. *Monthly Weather Review*, 148(11), 4545–4563. Retrieved 2022-07-20, from <https://journals.ametsoc.org/view/journals/mwre/148/11/MWR-D-20-0005.1.xml> doi: 10.1175/MWR-D-20-0005.1
- Davies, D. L., & Bouldin, D. W. (1979, April). A Cluster Separation Measure. *IEEE Transactions on Pattern Analysis and Machine Intelligence*, PAMI-1(2), 224–227. Retrieved 2022-05-16, from <http://ieeexplore.ieee.org/document/4766909/> doi: 10.1109/TPAMI.1979.4766909
- DeMaria, M., Franklin, J. L., Onderlinde, M. J., & Kaplan, J. (2021, May). Operational Forecasting of Tropical Cyclone Rapid Intensification at the National Hurricane Center. *Atmosphere*, 12(6), 683. Retrieved 2022-05-02, from <https://www.mdpi.com/2073-4433/12/6/683> doi: 10.3390/atmos12060683
- Demuth, J. L., DeMaria, M., Knaff, J. A., & Vonder Haar, T. H. (2004, February). Evaluation of Advanced Microwave Sounding Unit Tropical-Cyclone Intensity and Size Estimation Algorithms. *Journal of Applied Meteorology*, 43(2), 282–296. Retrieved 2022-07-20, from [http://journals.ametsoc.org/doi/10.1175/1520-0450\(2004\)043<0282:EOAMSU>2.0.CO;2](http://journals.ametsoc.org/doi/10.1175/1520-0450(2004)043<0282:EOAMSU>2.0.CO;2) doi: 10.1175/1520-0450(2004)043<0282:EOAMSU>2.0.CO;2
- Emanuel, K. (1989, November). The Finite-Amplitude Nature of Tropical Cyclogenesis. *Journal of the Atmospheric Sciences*, 46(22), 3431–3456. Retrieved 2022-06-29, from [http://journals.ametsoc.org/doi/10.1175/1520-0469\(1989\)046<3431:TFANOT>2.0.CO;2](http://journals.ametsoc.org/doi/10.1175/1520-0469(1989)046<3431:TFANOT>2.0.CO;2) doi: 10.1175/1520-0469(1989)046<3431:TFANOT>2.0.CO;2
- Emanuel, K. (2017, March). Will Global Warming Make Hurricane Forecasting More Difficult? *Bulletin of the American Meteorological Society*, 98(3), 495–501. Retrieved 2022-04-18, from <https://journals.ametsoc.org/doi/10.1175/BAMS-D-16-0134.1> doi: 10.1175/BAMS-D-16-0134.1
- Emanuel, K. (2018, January). 100 Years of Progress in Tropical Cyclone Research. *Meteorological Monographs*, 59, 15.1–15.68. Retrieved 2022-06-07, from <http://journals.ametsoc.org/doi/10.1175/AMSMONOGRAPHIS-D-18-0016.1> doi: 10.1175/AMSMONOGRAPHIS-D-18-0016.1
- Fischer, M. S., Rogers, R. F., & Reasor, P. D. (2020, March). The Rapid Intensification and Eyewall Replacement Cycles of Hurricane Irma (2017). *Monthly Weather Review*, 148(3), 981–1004. Retrieved 2022-07-20, from

- <http://journals.ametsoc.org/doi/10.1175/MWR-D-19-0185.1> doi:
10.1175/MWR-D-19-0185.1
- Guo, X., & Tan, Z.-M. (2017, May). Tropical cyclone fullness: A new concept for interpreting storm intensity: TROPICAL CYCLONE FULLNESS. *Geophysical Research Letters*, *44*(9), 4324–4331. Retrieved 2022-05-16, from <http://doi.wiley.com/10.1002/2017GL073680> doi: 10.1002/2017GL073680
- Hendricks, E. A., Peng, M. S., Fu, B., & Li, T. (2010, August). Quantifying Environmental Control on Tropical Cyclone Intensity Change. *Monthly Weather Review*, *138*(8), 3243–3271. Retrieved 2022-03-11, from <http://journals.ametsoc.org/doi/10.1175/2010MWR3185.1> doi: 10.1175/2010MWR3185.1
- Hersbach, H., Bell, B., Berrisford, P., Hirahara, S., Horányi, A., Muñoz-Sabater, J., ... Thépaut, J. (2020, July). The ERA5 global reanalysis. *Quarterly Journal of the Royal Meteorological Society*, *146*(730), 1999–2049. Retrieved 2022-05-04, from <https://onlinelibrary.wiley.com/doi/10.1002/qj.3803> doi: 10.1002/qj.3803
- Kaplan, J., & DeMaria, M. (2003, December). Large-Scale Characteristics of Rapidly Intensifying Tropical Cyclones in the North Atlantic Basin. *Weather and Forecasting*, *18*(6), 1093–1108. Retrieved 2022-03-11, from [http://journals.ametsoc.org/doi/10.1175/1520-0434\(2003\)018<1093:LCORIT>2.0.CO;2](http://journals.ametsoc.org/doi/10.1175/1520-0434(2003)018<1093:LCORIT>2.0.CO;2) doi: 10.1175/1520-0434(2003)018<1093:LCORIT>2.0.CO;2
- Kaplan, J., DeMaria, M., & Knaff, J. A. (2010, February). A Revised Tropical Cyclone Rapid Intensification Index for the Atlantic and Eastern North Pacific Basins. *Weather and Forecasting*, *25*(1), 220–241. Retrieved 2022-04-16, from <https://journals.ametsoc.org/doi/10.1175/2009WAF2222280.1> doi: 10.1175/2009WAF2222280.1
- Kaplan, J., Rozoff, C. M., DeMaria, M., Sampson, C. R., Kossin, J. P., Velden, C. S., ... Solbrig, J. E. (2015, October). Evaluating Environmental Impacts on Tropical Cyclone Rapid Intensification Predictability Utilizing Statistical Models. *Weather and Forecasting*, *30*(5), 1374–1396. Retrieved 2022-04-16, from <https://journals.ametsoc.org/doi/10.1175/WAF-D-15-0032.1> doi: 10.1175/WAF-D-15-0032.1
- Kieu, C. Q. (2012, January). An investigation into the contraction of the hurricane radius of maximum wind. *Meteorology and Atmospheric Physics*, *115*(1-2), 47–

56. Retrieved 2022-07-20, from <http://link.springer.com/10.1007/s00703-011-0171-7> doi: 10.1007/s00703-011-0171-7
- Knapp, K. R., Kruk, M. C., Levinson, D. H., Diamond, H. J., & Neumann, C. J. (2010, March). The International Best Track Archive for Climate Stewardship (IBTrACS): Unifying Tropical Cyclone Data. *Bulletin of the American Meteorological Society*, *91*(3), 363–376. Retrieved 2022-04-24, from <https://journals.ametsoc.org/doi/10.1175/2009BAMS2755.1> doi: 10.1175/2009BAMS2755.1
- Kohonen, T. (1990, September). The self-organizing map. *Proceedings of the IEEE*, *78*(9), 1464–1480. Retrieved 2022-07-06, from <http://ieeexplore.ieee.org/document/58325/> doi: 10.1109/5.58325
- Kohonen, T. (2013, January). Essentials of the self-organizing map. *Neural Networks*, *37*, 52–65. Retrieved 2022-07-06, from <https://linkinghub.elsevier.com/retrieve/pii/S0893608012002596> doi: 10.1016/j.neunet.2012.09.018
- Kowch, R., & Emanuel, K. (2015, March). Are Special Processes at Work in the Rapid Intensification of Tropical Cyclones? *Monthly Weather Review*, *143*(3), 878–882. Retrieved 2022-07-06, from <http://journals.ametsoc.org/doi/10.1175/MWR-D-14-00360.1> doi: 10.1175/MWR-D-14-00360.1
- Landsea, C. W. (2022, April). *The revised Northeast and North Central Pacific hurricane database (HURDAT2)*. Retrieved from <https://www.nhc.noaa.gov/data/hurdat/hurdat2-format-nencpac-1949-2021.pdf>
- Lee, C.-Y., Tippett, M. K., Sobel, A. H., & Camargo, S. J. (2016, April). Rapid intensification and the bimodal distribution of tropical cyclone intensity. *Nature Communications*, *7*(1), 10625. Retrieved 2022-03-12, from <http://www.nature.com/articles/ncomms10625> doi: 10.1038/ncomms10625
- Li, Y., Tang, Y., & Wang, S. (2022, July). Rapid Growth of Outer Size of Tropical Cyclones: A New Perspective on Their Destructive Potential. *Geophysical Research Letters*, *49*(13). Retrieved 2022-06-30, from <https://onlinelibrary.wiley.com/doi/10.1029/2022GL099230> doi: 10.1029/2022GL099230
- Li, Y., Wang, Y., & Lin, Y. (2019, October). Revisiting the Dynamics of Eye-wall Contraction of Tropical Cyclones. *Journal of the Atmospheric Sciences*, *76*(10), 3229–3245. Retrieved 2022-03-02, from <https://journals.ametsoc.org/doi/10.1175/JAS-D-19-0076.1> doi: 10.1175/JAS-D-19-0076.1

- Li, Y., Wang, Y., Lin, Y., & Wang, X. (2021, August). Why does rapid contraction of the radius of maximum wind precede rapid intensification in tropical cyclones? *Journal of the Atmospheric Sciences*. Retrieved 2022-03-11, from <https://journals.ametsoc.org/view/journals/atsc/aop/JAS-D-21-0129.1/JAS-D-21-0129.1.xml> doi: 10.1175/JAS-D-21-0129.1
- Li, Y., Wang, Y., & Tan, Z.-M. (2022, April). How frequently does rapid intensification occur after rapid contraction of the radius of maximum wind in tropical cyclones over the North Atlantic and Eastern North Pacific? *Monthly Weather Review*. Retrieved 2022-07-02, from <https://journals.ametsoc.org/view/journals/mwre/aop/MWR-D-21-0322.1/MWR-D-21-0322.1.xml> doi: 10.1175/MWR-D-21-0322.1
- Liu, Y., Weisberg, R. H., & Mooers, C. N. K. (2006). Performance evaluation of the self-organizing map for feature extraction. *Journal of Geophysical Research*, 111(C5), C05018. Retrieved 2022-07-06, from <http://doi.wiley.com/10.1029/2005JC003117> doi: 10.1029/2005JC003117
- Ma, Z., Fei, J., & Huang, X. (2019, October). A Definition of Rapid Weakening for Tropical Cyclones Over the Western North Pacific. *Geophysical Research Letters*, 46(20), 11471–11478. Retrieved 2022-05-06, from <https://onlinelibrary.wiley.com/doi/10.1029/2019GL085090> doi: 10.1029/2019GL085090
- Mallen, K. J., Montgomery, M. T., & Wang, B. (2005, February). Reexamining the Near-Core Radial Structure of the Tropical Cyclone Primary Circulation: Implications for Vortex Resiliency. *Journal of the Atmospheric Sciences*, 62(2), 408–425. Retrieved 2022-06-29, from <https://journals.ametsoc.org/doi/10.1175/JAS-3377.1> doi: 10.1175/JAS-3377.1
- Montgomery, M., & Smith, R. (2014, March). Paradigms for tropical cyclone intensification. *Australian Meteorological and Oceanographic Journal*, 64(1), 37–66. Retrieved 2022-04-29, from <http://www.bom.gov.au/jshess/docs/2014/montgomery.pdf> doi: 10.22499/2.6401.005
- Qin, N., Zhang, D., Miller, W., & Kieu, C. Q. (2018, October). On the rapid intensification of Hurricane *Wilma* (2005). Part IV: Inner-core dynamics during the steady radius of maximum wind stage. *Quarterly Journal of the Royal Meteorological Society*, 144(717), 2508–2523. Retrieved 2022-07-20,

- from <https://onlinelibrary.wiley.com/doi/10.1002/qj.3339> doi:
10.1002/qj.3339
- Rappaport, E. N., Jiing, J.-G., Landsea, C. W., Murillo, S. T., & Franklin, J. L. (2012, March). The Joint Hurricane Test Bed: Its First Decade of Tropical Cyclone Research-To-Operations Activities Reviewed. *Bulletin of the American Meteorological Society*, *93*(3), 371–380. Retrieved 2022-04-16, from <https://journals.ametsoc.org/doi/10.1175/BAMS-D-11-00037.1> doi: 10.1175/BAMS-D-11-00037.1
- Rogers, R., Aberson, S., Aksoy, A., Annane, B., Black, M., Cione, J., . . . Zhang, X. (2013, June). NOAA'S Hurricane Intensity Forecasting Experiment: A Progress Report. *Bulletin of the American Meteorological Society*, *94*(6), 859–882. Retrieved 2022-06-29, from <https://journals.ametsoc.org/doi/10.1175/BAMS-D-12-00089.1> doi: 10.1175/BAMS-D-12-00089.1
- Rousseeuw, P. J. (1987, November). Silhouettes: A graphical aid to the interpretation and validation of cluster analysis. *Journal of Computational and Applied Mathematics*, *20*, 53–65. Retrieved 2022-05-16, from <https://linkinghub.elsevier.com/retrieve/pii/0377042787901257> doi: 10.1016/0377-0427(87)90125-7
- Schubert, W. H., & Hack, J. J. (1982, August). Inertial Stability and Tropical Cyclone Development. *Journal of the Atmospheric Sciences*, *39*(8), 1687–1697. Retrieved 2022-06-29, from [http://journals.ametsoc.org/doi/10.1175/1520-0469\(1982\)039<1687:ISATCD>2.0.CO;2](http://journals.ametsoc.org/doi/10.1175/1520-0469(1982)039<1687:ISATCD>2.0.CO;2) doi: 10.1175/1520-0469(1982)039<1687:ISATCD>2.0.CO;2
- Shapiro, L. J., & Willoughby, H. E. (1982, February). The Response of Balanced Hurricanes to Local Sources of Heat and Momentum. *Journal of the Atmospheric Sciences*, *39*(2), 378–394. Retrieved 2022-06-29, from [http://journals.ametsoc.org/doi/10.1175/1520-0469\(1982\)039<0378:TROBHT>2.0.CO;2](http://journals.ametsoc.org/doi/10.1175/1520-0469(1982)039<0378:TROBHT>2.0.CO;2) doi: 10.1175/1520-0469(1982)039<0378:TROBHT>2.0.CO;2
- Sitkowski, M., Kossin, J. P., & Rozoff, C. M. (2011, December). Intensity and Structure Changes during Hurricane Eyewall Replacement Cycles. *Monthly Weather Review*, *139*(12), 3829–3847. Retrieved 2022-07-20, from <http://journals.ametsoc.org/doi/10.1175/MWR-D-11-00034.1> doi: 10.1175/MWR-D-11-00034.1

- Stern, D. P., Vigh, J. L., Nolan, D. S., & Zhang, F. (2015, April). Revisiting the Relationship between Eyewall Contraction and Intensification. *Journal of the Atmospheric Sciences*, *72*(4), 1283–1306. Retrieved 2022-04-29, from <https://journals.ametsoc.org/doi/10.1175/JAS-D-14-0261.1> doi: 10.1175/JAS-D-14-0261.1
- Vigh, J. L., Knaff, J. A., & Schubert, W. H. (2012, May). A Climatology of Hurricane Eye Formation. *Monthly Weather Review*, *140*(5), 1405–1426. Retrieved 2022-07-20, from <https://journals.ametsoc.org/doi/10.1175/MWR-D-11-00108.1> doi: 10.1175/MWR-D-11-00108.1
- Wang, Y., Li, Y., Xu, J., Tan, Z.-M., & Lin, Y. (2021, April). The Intensity-dependence of Tropical Cyclone Intensification Rate in a Simplified Energetically Based Dynamical System Model. *Journal of the Atmospheric Sciences*. Retrieved 2022-03-02, from <https://journals.ametsoc.org/view/journals/atsc/aop/JAS-D-20-0393.1/JAS-D-20-0393.1.xml> doi: 10.1175/JAS-D-20-0393.1
- Wang, Y., & Wu, C.-C. (2004, December). Current understanding of tropical cyclone structure and intensity changes ? a review. *Meteorology and Atmospheric Physics*, *87*(4), 257–278. Retrieved 2022-04-29, from <http://link.springer.com/10.1007/s00703-003-0055-6> doi: 10.1007/s00703-003-0055-6
- Wang, Y.-F., & Tan, Z.-M. (2020). Outer Rainbands–Driven Secondary Eyewall Formation of Tropical Cyclones. *JOURNAL OF THE ATMOSPHERIC SCIENCES*, *77*, 20.
- Wu, L., Zhao, H., Wang, C., Cao, J., & Liang, J. (2022, February). Understanding of the Effect of Climate Change on Tropical Cyclone Intensity: A Review. *Advances in Atmospheric Sciences*, *39*(2), 205–221. Retrieved 2022-06-29, from <https://link.springer.com/10.1007/s00376-021-1026-x> doi: 10.1007/s00376-021-1026-x
- Wu, Q., & Ruan, Z. (2021, February). Rapid Contraction of the Radius of Maximum Tangential Wind and Rapid Intensification of a Tropical Cyclone. *Journal of Geophysical Research: Atmospheres*, *126*(3). Retrieved 2022-03-11, from <https://onlinelibrary.wiley.com/doi/10.1029/2020JD033681> doi: 10.1029/2020JD033681
- Xu, J., & Wang, Y. (2015, June). A Statistical Analysis on the Dependence of Trop-

ical Cyclone Intensification Rate on the Storm Intensity and Size in the North Atlantic. *Weather and Forecasting*, 30(3), 692–701. Retrieved 2022-06-29, from <https://journals.ametsoc.org/doi/10.1175/WAF-D-14-00141.1> doi: 10.1175/WAF-D-14-00141.1

Xu, J., & Wang, Y. (2018, April). Dependence of Tropical Cyclone Intensification Rate on Sea Surface Temperature, Storm Intensity, and Size in the Western North Pacific. *Weather and Forecasting*, 33(2), 523–537. Retrieved 2022-06-29, from <https://journals.ametsoc.org/doi/10.1175/WAF-D-17-0095.1> doi: 10.1175/WAF-D-17-0095.1

Xu, J., Wang, Y., & Tan, Z.-M. (2016, December). The Relationship between Sea Surface Temperature and Maximum Intensification Rate of Tropical Cyclones in the North Atlantic. *Journal of the Atmospheric Sciences*, 73(12), 4979–4988. Retrieved 2022-06-29, from <https://journals.ametsoc.org/doi/10.1175/JAS-D-16-0164.1> doi: 10.1175/JAS-D-16-0164.1